Batteries & Supercaps

Research Article
doi.org/10.1002/batt.202300126

Chemistry Europe
European Chemical Societies Publishing

www.batteries-supercaps.org

Elucidating Degradation Mechanisms of Silicon-graphite Electrodes in Lithium-ion Batteries by Local Electrochemistry

Nomnotho Jiyane,[a] Enrique García-Quismondo,[b] Edgar Ventosa,[c] Wolfgang Schuhmann,*[a] and Carla Santana Santos*[a]

The integrity of the solid electrolyte interphase (SEI) formed on the negative electrode of lithium-ion batteries (LIB) is especially critical for the performance of next-generation LIBs comprising silicon-carbon based electrode materials. The protecting character of the SEI is compromised due to volume expansion and shrinking during de/intercalation of Li ions leading to irreversible changes upon long-term cycling. Scanning electrochemical microscopy (SECM) is proposed as local electrochemical technique to investigate the degradation mechanisms of advanced negative electrodes. The impact of charge/discharge cycling on the SEI properties on Si–C electrodes was investigated, and the sensitivity of SECM successfully reveals inhomogeneities at an early stage of the cycling already at about 5 cycles. Macroscopic EIS measurements and evaluation of the coulombic efficiency may result in misleading interpretations of degradation. SECM is demonstrated to be a powerful and complementary technique for revealing μm-heterogeneities in the SEI surface reactivity after a few charge/discharge cycles.

Introduction

Graphite remains the most widely used material for negative electrodes in lithium-ion batteries (LIB) due to its long cycle life, low operating voltage, and cost-effectiveness.[1] New alternative materials are of utmost importance to improve battery capacity, sustainability, and costs. One of the promising materials is silicon, often mixed with carbon, which is considered a next-generation LIB material due to its high theoretical specific capacity of 4200 mAh g^{-1}, the abundance of Si on earth, and the high Li-ion diffusivity in amorphous α-Li_xSi.[2–4] Due to the formation of a Li–Si alloy Si suffers from a large volume change during lithiation/de-lithiation in consecutive charge-discharge cycles. The concomitant morphological changes lead to physical distortions provoking defects in the anode material, thus affecting the stability of the SEI.[5–7] The SEI is a nanometre-thick protecting film,[8] which is electronically insulating and ionically conducting, preventing continuous electrolyte decomposition at the electrode surface.[9] This protective property enables the achieved long cycle life of LIB, although the negative electrodes operate far away from the stability window of the electrolyte. Therefore, stability and integrity of the SEI have been identified as the main limitation for the Si-based LIB electrodes due to the volume changes occurring upon (de-)lithiation. [10,11]

A variety of different methods were applied to gain fundamental insight into the morphology and chemical composition of the SEI, namely X-ray absorption spectroscopy (XAS),[12] X-ray photoelectron spectroscopy (XPS),[13] energy-dispersive X-ray spectroscopy (EDX),[14] atomic force microscopy (AFM),[15] and scanning electron microscopy (SEM).[16–19] Electrochemical impedance spectroscopy (EIS) is the most widely used method to evaluate the electrochemical properties of the SEI.[20,21] While much attention is paid to assessing the ionic properties of the SEI by EIS, the protecting properties of the SEI caused by negligible electronic conductivity are rarely investigated, most likely due to a lack of simple but suitable analytical tools.[22] Scanning electrochemical probe microscopy techniques were demonstrated as a powerful in-*situ* approach to uncover the electrochemical properties of the SEI with a lateral resolution in the μm-nm range.[23] The so-called feedback mode of scanning electrochemical microscopy (SECM) is able to interrogate the local electrochemical reactivity of the SEI and to locally map the electron transfer kinetics across the SEI.[24–28] SECM was used to investigate the surface reactivity of Si electrodes.[29,30] However, while useful insight into the surface reactivity of model Si samples were disclosed, the behavior and

[a] *N. Jiyane, Prof. Dr. W. Schuhmann, Dr. C. S. Santos*
Analytical Chemistry- Center for Electrochemical Sciences (CES)
Faculty of Chemistry and Biochemistry
Ruhr-Universität Bochum
Universitätstrasse 150, 44780 Bochum (Germany)
E-mail: wolfgang.schuhmann@rub.de
carla.santanasantos@rub.de

[b] *Dr. E. García-Quismondo*
Electrochemical Processes Unit
IMDEA Energy Institute
Avda. Ramón de la Sagra 3, 28935 Mòstoles (Spain)

[c] *Prof. Dr. E. Ventosa*
Department of Chemistry
University of Burgos
Pza. Miseal Bañuelos s/n, E-09001 Burgos (Spain)

Supporting information for this article is available on the WWW under https://doi.org/10.1002/batt.202300126

Research Article
doi.org/10.1002/batt.202300126
Chemistry Europe
European Chemical Societies Publishing

challenges of *real-world* porous Si-based electrodes may differ significantly. To the best of our knowledge, feedback-mode SECM (FB-SECM) was not reported for the investigation of the SEI properties on commercial silicon or silicon-graphite (Si–C) surfaces, despite the evolution of the integrity of the SEI is known to be critical for the performance of Si-based electrodes.

Herein, FB-SECM is applied as an accelerated approach to investigate the degradation of commercial and porous Si-graphite electrodes. SEI-covered Si–C samples were systematically prepared by electrochemical ageing of individual Si–C electrodes using a coaxial three-electrode configuration Swagelok cell [31] to ensure reproducibility. After disassembling the cell inside the argon-filled glovebox, the SEI-covered S–C electrode was interrogated using FB-SECM demonstrating the formation of inhomogeneities in the SEI already after a few charge-discharge cycles.

Results and Discussion

SEI formation on commercial Si–C electrodes

Electrochemical ageing of Si–C electrodes was performed using a previously described coaxial three-electrode Swagelok cell[31,32] and a cyclic potentiodynamic protocol. The three-electrode configuration is essential to ensure potential control between the working electrode (anode) and the reference electrode (Li) while the current flows through the counter electrode (Li disc). Moreover, before disassembling, the aged electrodes were characterized through EIS. Using the coaxial cell configuration (see scheme in Figure 1a) allows us to mitigate artefacts which appear in conventional three-electrode Swagelok T-cells due to the lack of symmetric current lines.[31] Differences in the impact of the design of the Swagelok cells on the EIS are discussed in more detail in the Supporting Information (Section S1).

The formation of the SEI was carried out by scanning the potential of the pristine Si–C electrode from the open-circuit potential (OCP) until 10 mV vs. Li/Li^+. Samples with varying ageing states were prepared by scanning the potential from 10 mV to 1.5 V at a scan rate of 0.1 $mV\,s^{-1}$ after the initial SEI formation to provoke Li^+ de-intercalation. The number of potentiodynamic cycles was 1, 3, 5, 7, 9, and 11. Note, that each sample was prepared with a new pristine Si–C anode.

The evolution of coulombic efficiency (CE) with the number of potentiodynamic cycles after SEI formation is shown in Figure 1(b); for more details, see Supporting Information, Section S2. The CE steadily increased during the first cycles until cycle number 7 and remained nearly stable at 95 % until cycle 11. The Nyquist plots of the corresponding potentiostatic EIS measurements for the lithiated negative electrodes are displayed in Figure 1(c). The charge transfer resistance (R_{ct}) and the SEI resistance (R_{SEI}) were derived by fitting the experimental EIS data to electrical equivalent circuits. Interestingly, after the first cycle, a clear contribution of the SEI was noticed with the appearance of an RC process. After cycles 3, 5 and 7 a higher internal resistance appeared, with a clear one-RC contribution. This is attributed to the overlap of time constants for both charge-transfer processes leading to the resistances, R_{SEI} and R_{ct}. The analysis of EIS data showed the evolution of the areal resistance, namely the sum of resistances (electrolyte, SEI, and charge transfer resistances, $R_e + R_{SEI} + R_{ct}$). The internal resistance increased with the number of cycles, i.e., the value of $R_e + R_{SEI} + R_{ct}$ increased from 28.7 Ω, to 40.4 Ω, to 46.3 Ω, to 52.0 Ω, to 66.0 Ω, to 108.3 Ω for 1 cycle, 3 cycles, 5 cycles, 7 cycles, 9 cycles and 11 cycles, respectively. Notice that the Nyquist plots obtained from the samples with 9 and 11 cycles exhibit two separate charge-transfer processes. Despite the EIS data unambiguously revealing a correlation between the internal resistance and the capacity fading during cycling, without additional insights into the degradation process, an in-depth interpretation of the EIS measurements is impossible. The evolution of the CE becoming stable after 7 cycles cannot explain the EIS data. Ageing of Si–C electrodes is used to illustrate the need for complementary electrochemical techniques for a deeper interpretation of the complex electrochemical reactions occurring in real-world electrodes.

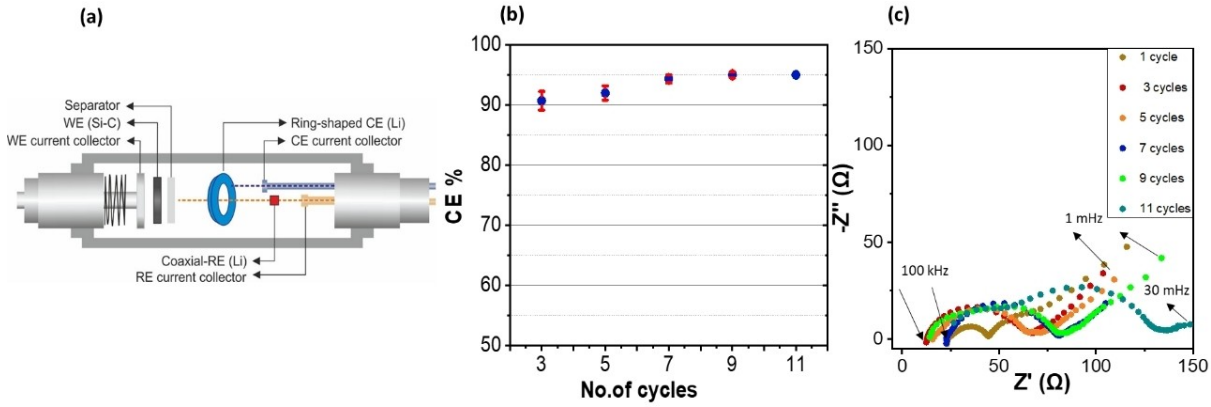

Figure 1. a) Scheme of the coaxial-Swagelok cell (three electrodes).[32] b) Coulombic efficiency (mean and standard error of the means) of each cycled Si–C sample. c) Nyquist plots of Si–C electrodes after cycling at OCP; EIS were recorded using the coaxial-Swagelok cell. Electrolyte: 1 M $LiPF_6$ (EC: DMC) + VC 2 %*w/w*. EIS performed at DC: OCP, AC: 10 mV rms, frequency range: 100 kHz to 1 mHz.

Research Article
doi.org/10.1002/batt.202300126
Chemistry Europe
European Chemical Societies Publishing

Local electrochemistry of cycled Si-C electrodes

Feedback mode SECM (FB-SECM) was employed to investigate Si–C electrodes at different ageing stages. Each Si–C electrode was transferred from the Swagelok cell into the SECM cell. To avoid any contamination of the samples, SECM measurements were carried out inside the same Ar-filled glovebox (for more experimental details see Supporting Information, Section S3). The SECM cell was filled with a battery-grade electrolyte consisting of 1 M $LiClO_4$ in EC:PC in the presence of ferrocene (Fc) as a redox mediator. Note that electrochemical ageing in the Swagelok cell was carried out using a standard battery electrolyte. The SECM tip (Pt-disc ultramicroelectrode, 25 μm) was biased to 3.5 V vs. Li/Li^+ for the oxidation of Fc. The sample electrode surface was not polarized during the SECM evaluation. The tip response correlates with the capability of the sample surface to promote electron transfer reactions so that the protecting character of the SEI towards electrolyte decomposition can be interrogated.

Figure 2 shows SECM maps over Si–C electrodes aged with different cycle numbers. The normalized current responses indicated a homogeneous reactive surface over the pristine sample ($i/i_{bulk} > 1$, Figure 2a). In contrast, a heterogeneous SECM map was recorded over the electrode after SEI formation without further cycling (Figure 2b). Some regions showed an $i/i_{bulk} \gg 1$ (orange), which represents an interface capable of promoting electron transfer reactions at a high rate, while there were some regions where the surface showed a protecting character ($i/i_{bulk} \ll 1$, greenish), which is attributed to an SEI-covered surface. The orange areas are obviously not protected by an intact SEI. The overall surface area scanned by the SECM tip was typically $1 \times 1\ mm^2$, and the SEI-protected zones in Figure 1(b) were in the μm^2 scale range. The SEI-covered area increased with the number of cycles, as clearly seen in the SECM maps recorded over the Si–C samples after 3 and 5 cycles (Figure 2c and 2d, respectively). The number of reactive pixels increased in the SECM image of the sample after 7 cycles (Figure 2e), indicating that repetitive cycling provokes a loss of protecting character. Although the SECM imaging was only performed over a comparatively small area, it is reasonable to believe that the size of the area is sufficiently representative of the entire electrode surface. With the number of cycles, the protecting character of the SEI diminished continuously from 5 to 11 cycles (Figure 2d–g). After 11 cycles the protecting character of the SEI was lost. Figure 2(h) shows the statistics of the normalized current for each SECM map indicating the heterogeneity in each sample. The average values of i/i_{bulk} decreased with the increasing number of cycles until cycle number 5, suggesting an increasing protecting character of the SEI with the number of cycles. Afterwards, from cycle 5 on, the average values of i/i_{bulk} increased, indicating a decrease in the protecting character of the SEI. However, the trend for the last cycles does not correlate with the macroscopic results. While the capacity was continuously fading, the coulombic efficiency remained stable after 5 cycles. This discrepancy indicates a second influencing factor. We suggest that the volume changes inherent to charging/discharging of Si–C electrodes lead to the detachment of active particles. This detachment would expose SEI-uncovered areas. SECM mapping indicates that while the SEI quickly improve its protecting character, detachment of active materials plays a significant role at higher cycle numbers. Besides the intuitive information provided by SECM surface mapping, intrinsic properties of the surface, such as quantitative kinetic parameters, can be extracted by performing approach curves of the polarized microelectrode tip towards the surface. The shape of the normalized approach curve is dependent on

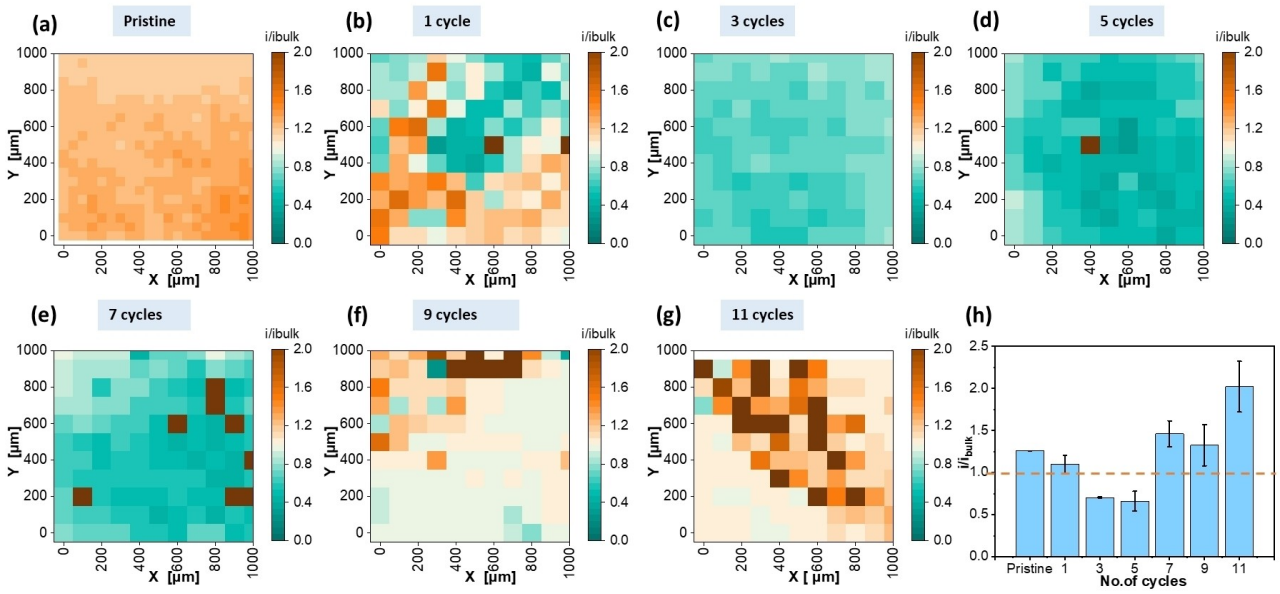

Figure 2. SECM maps of Si–C electrode samples, a–g) scanned region on Si–C surfaces showing areas covered with SEI with values of $i/i_{bulk} < 1$ (green) representing insulating properties, and $i/i_{bulk} > 1$ (orange) indicating conductive properties. Measurements were performed in 10 mM Fc; 1 M $LiClO_4$ (EC: PC); E_{tip} 3.5 V vs. Li. h) bar graph showing the average of all current values of an SECM map; error bars represent the standard deviation for each SECM image.

Research Article
doi.org/10.1002/batt.202300126
Chemistry Europe
European Chemical Societies Publishing

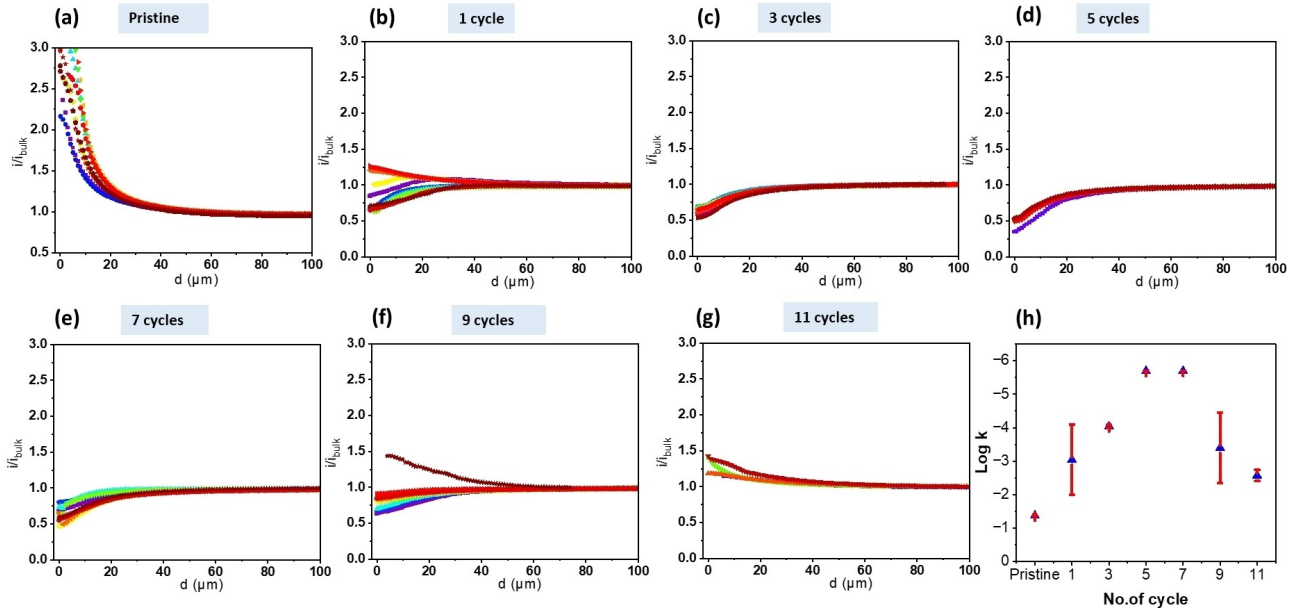

Figure 3. a–g) FB-SECM approach curves: dimensionless plots (i/i_{bulk} vs. d) showing the tip current as a function of tip-to-surface distance. SECM tip: 25 μm Pt UME, electrolyte: 10 mM FC in 1 M $LiClO_4$ (EC: PC). Each approach curve was performed at different locations 100 μm apart from each other. h) Mean k-value in dependence from the cycle number

the SECM tip geometry, which is known, and the first-order kinetics rate constants, k (cm/s), of the Fc^+ reduction process occurring at the sample surface. Quantitative kinetics values were obtained by fitting the approach curves to the theoretical expressions.[33] In general, a fast electron-transfer reaction at a conducting surface exhibits $k \rightarrow \infty$, while at a completely insulating surface $k \rightarrow 0$. Sequential approach curves were recorded at different locations over the same electrode samples, and the k-values were derived by fitting. The FB-SECM approach curves are shown in Figure 3 and the corresponding k-values are summarized in Figure 3(h) and Table S3 in the Supporting Information. For approach curves performed towards the pristine Si–C surface (log $k = -1.4$), the normalized current increased in the vicinity of the substrate due to positive feedback. [26,34] In agreement with the SECM maps, the approach curves towards a Si–C surface after SEI formation presented a heterogenous response (Figure 3b).

There were regions with protecting characteristics indicating the formation of an effective SEI, and some areas revealed high electron-transfer rates due to a poorly protecting SEI or a not-SEI covered surface. The calculated k values (log $k = -3$) are lower than those obtained for the pristine surface.

A negative feedback effect was observed for the approach curves performed towards the electrode samples after 3, 5 and 7 cycles (Figure 3c–e). The rate constant decreased to log $k = -6$, confirming the presence of a homogeneous and effectively protecting SEI. The approach curves towards the electrode sample after 9 cycles revealed various areas with effective protecting and poorly protecting properties with a wide variation of the electron-transfer rate constant (Figure 3h). After 11 cycles, a non-protecting electrode surface with a log $k = -2.5$ was obtained. Our previous results for model thin-film Si electrodes revealed that the SEI was already damaged during the first delithiation due to volume changes.[29] The formed discontinuities in the SEI were "covered" by fresh SEI formed during the second lithiation so that a homogeneous SEI was obtained after 3 cycles. This is consistent with the results obtained for commercial Si–C electrodes. However, due to the likely detachment of active particles upon prolonged cycling, SEI-uncovered areas are exposed. Hence, as suggested by the SECM results, on the one hand, the surface reactivity and on the other hand, the charge-transfer resistance for the (de-)lithiation process increase explaining the global EIS data shown above. Figure 4 summarizes schematically the proposed ageing mech-

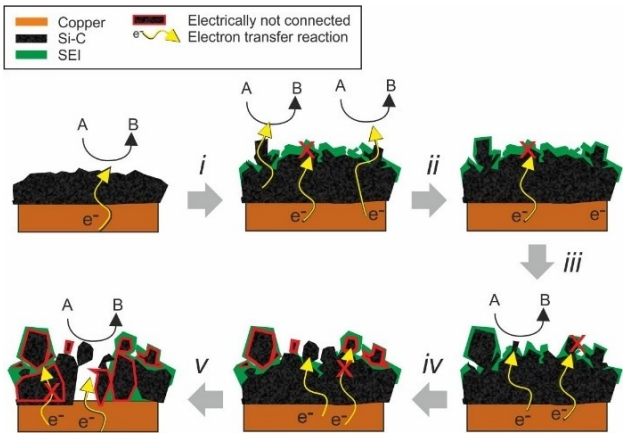

Figure 4. Illustration of proposed degradation mechanism for commercial Si–C electrodes. Initially, SEI growth is heterogeneous, and regions with large variations in the protecting properties of the SEI are obtained (i, ii). With increasing cycle number, a more homogeneous SEI is obtained (iii). Prolonged cycling causes cracking (iv) and, ultimately, disintegration (v) of the anode material.

anism. Figure 4(i) shows the initial SEI formation, and after 3 cycles the formed SEI blocked the electron-transfer reaction at the surface (Figure 4ii). Figure 4(iii and iv) shows the appearance of not SEI-covered regions leading ultimately to a detachment of Si–C particles (Figure 4v).

Conclusions

Elucidation of degradation mechanisms for next-generation LIB electrodes in which unknown processes are taking place simultaneously requires the implementation of complementary analytical techniques. Commercial Si-graphite electrodes were used in this work as a case study to illustrate the capability of SECM to complement EIS. The evaluation of the evolution of surface reactivity at the Si–C electrodes during the cycling processes by means of FB-SECM measurements unraveled two major ageing processes. Firstly, the formation of an effective SEI was observed, which became more homogeneous during the first few cycles. The heterogeneous electron-transfer rate constant *k* derived from SECM approach curves decreased significantly during these first cycles. Prolonged cycling led to the appearance of areas with high *k* values due to the detachment of active particles. The information revealed by FB-SECM provided the basis for the interpretation of the evolution of global EIS results. SECM was demonstrated as a complementary characterization technique for real-world commercial electrodes, which contributes to the interpretation of complex electrochemical processes as illustrated for the case of next-generation Si-based electrodes.

Experimental Section

Chemical and electrode material

All chemicals and reagents were used as received from the manufacturer. 99.9% Lithium ribbon 0.38 mm thick, battery-grade lithium hexafluorophosphate solution in ethylene carbonate and dimethyl carbonate (1.0 M $LiPF_6$ in EC: DMC (v/v)) were from Sigma–Aldrich. Ferrocene (Fc) (98%), ethylene carbonate (EC), propylene carbonate (PC) 99.7% anhydrous, and vinylene carbonate (VC), were obtained from Sigma–Aldrich and 98% Lithium perchlorate, $LiClO_4$, from Alfa Aesar. 0.025 mm 99.9% Pt wire was purchased from Goodfellow and sealed in borosilicate glass capillary 100 mm, outside ø 1.5 mm (Hilgenberg). Ti mesh was used as coaxial counter electrode (CE). All experiments were performed using an Autolab potentiostat PGSTAT 30.

Negative electrode

The vacuum-sealed pouch cell (Si–C 15%, NMC 811 composition) was from LiFun Technology and used as received without electrolyte (dry). The negative electrode was disassembled inside the glovebox and cut with a spherical puncher prior to the cycling process. SEI formation was performed using a standard three-electrode Swagelok cell, commonly used in LIBs. Figure S1(a) in the Supporting Information displays a representation of the T-cell. The circular punched-off battery electrode and Li metal (10 mm) were used as WE and CE, respectively. Additionally, a polyolefin membrane was used to avoid damage to the SEI upon disassembling the cell, along with a glass fibre separator to carry 100 µL 1 M $LiPF_6$ EC: DMC (1:1 wt%) 2% VC w/w. A thin concave reference electrode (RE) (6 mm ø) filled with a small Li metal strip was placed in the cell, and an additional glass fibre separator soaked with 50 µL SEI electrolyte was placed between the electrode sandwich and the reference electrode.

The coaxial Swagelok cell has a RE in a coaxial position in the plane with the annular WE.[32] The CE was Li ribbon (12 mm ø), and the WE was the Si–C substrate (12 mm ø). Polyolefin and glass fibre separators (12 mm ø) wetted with 80 µL $LiPF_6$ 2% VC w/w electrolyte were used to separate the CE and the WE.

Electrochemical measurements

Electrochemical impedance spectroscopy (EIS) was carried out on pristine samples and after cycling at a DC potential of around 2.1 V and 0.1 V, respectively. In the coaxial Swagelok cell, the frequency range for EIS measurement was 100 kHz to 1 mHz. Potentiodynamic charging was performed at individual pristine Si–C sample surfaces by scanning the potential from open circuit potential (OCP) to 0.01 V vs. Li/Li^+. Linear sweep voltammograms were performed at a scan rate of 0.1 $mV\,s^{-1}$ followed by holding the potential at 10 mV for 1 hour to grow the SEI. After that, the potential was cycled from 10 mV to 1.5 V (cycling). Lastly, another global EIS measurement was carried out with the charged anode (DC potential of around 100 mV). Scanning electrochemical microscopy was carried out using an in-house setup inside an Ar-filled glovebox ($O_2 < 0.1$ ppm, $H_2O < 0.1$ ppm). FB-SECM and imaging were performed in a 10 mM ferrocene (Fc) solution dissolved with 1 M $LiClO_4$ ethylene carbonate (EC) and propylene carbonate (PC) 1:1 containing 1 M $LiClO_4$ in the dedicated SECM electrochemical cell.

Supporting Information

Additional references cited within the Supporting Information.[32,33,35,36]

Acknowledgements

The authors are grateful for the financial support from the European Union's Horizon 2020 research and innovation program under the grant agreement NanoBat No. 861962. Open Access funding enabled and organized by Projekt DEAL.

Conflict of Interests

The authors declare no conflict of interest.

Data Availability Statement

The data that support the findings of this study are available from the corresponding author upon reasonable request.

Keywords: lithium-ion battery · electron transfer kinetics · Si–C · scanning electrochemical microscopy · solid electrolyte interphase

[1] D. Hu, L. Chen, J. Tian, Y. Su, N. Li, G. Chen, Y. Hu, Y. Dou, S. Chen, F. Wu, *Chin. J. Chem.* **2021**, *39*, 165–173.
[2] J. Wu, Y. Cao, H. Zhao, J. Mao, Z. Guo, *Carbon Energy* **2019**, *1*, 57–76.
[3] a) E. dos Santos Sardinha, M. Sternad, H. M. R. Wilkening, G. Wittstock, *ACS Appl. Energ. Mater.* **2019**, *2*, 1388–1392; b) J. Tan, J. Matz, P. Dong, J. Shen, M. Ye, *Adv. Energy Mater.* **2021**, *11*, 2100046.
[4] A. Majid, A. Fatima, S. U.-D. Khan, S. Khan, *New J. Chem.* **2021**, *45*, 19105–19117.
[5] V. A. Agubra, J. W. Fergus, *J. Power Sources* **2014**, *268*, 153–162.
[6] Y. Li, M. Liu, X. Feng, Y. Li, F. Wu, Y. Bai, C. Wu, *ACS Energy Lett.* **2021**, *6*, 3307–3320.
[7] H. B. Chew, B. Hou, X. Wang, S. Xia, *Int. J. Solids Struct.* **2014**, *51*, 4176–4187.
[8] P. Verma, P. Maire, P. Novák, *Electrochim. Acta* **2010**, *55*, 6332–6341.
[9] J. Zhou, K. Ma, X. Lian, Q. Shi, J. Wang, Z. Chen, L. Guo, Y. Liu, A. Bachmatiuk, J. Sun, R. Yang, J.-H. Choi, M. H. Rümmeli, *Small* **2022**, *18*, e2107460.
[10] M. N. Obrovac, V. L. Chevrier, *Chem. Rev.* **2014**, *114*, 11444–11502.
[11] a) D. Ma, Z. Cao, A. Hu, *Nano-Micro Lett.* **2014**, *6*, 347–358; b) S. Chae, M. Ko, K. Kim, K. Ahn, J. Cho, *Joule* **2017**, *1*, 47–60.
[12] M. Schellenberger, R. Golnak, W. G. Quevedo Garzon, S. Risse, R. Seidel, *Mater. Today* **2022**, *14*, 100215.
[13] M. Nie, D. P. Abraham, Y. Chen, A. Bose, B. L. Lucht, *J. Phys. Chem. C* **2013**, *117*, 13403–13412.
[14] I. Dienwiebel, M. Winter, M. Börner, *J. Phys. Chem. C* **2022**, *126*, 11016–11025.
[15] R. Kumar, A. Tokranov, B. W. Sheldon, X. Xiao, Z. Huang, C. Li, T. Mueller, *ACS Energy Lett.* **2016**, *1*, 689–697.
[16] M. Su, Z. Wang, H. Guo, X. Li, S. Huang, L. Gan, W. Xiao, *Powder Technol.* **2013**, *249*, 105–109.
[17] Y. Li, K. Leung, Y. Qi, *Acc. Chem. Res.* **2016**, *49*, 2363–2370.
[18] D. Diddens, W. A. Appiah, Y. Mabrouk, A. Heuer, T. Vegge, A. Bhowmik, *Adv. Mater. Interfaces* **2022**, *9*, 2101734.
[19] A. Wang, S. Kadam, H. Li, S. Shi, Y. Qi, *npj Comput. Mater.* **2018**, *4*, 1–26.
[20] N. Meddings, M. Heinrich, F. Overney, J.-S. Lee, V. Ruiz, E. Napolitano, S. Seitz, G. Hinds, R. Raccichini, M. Gaberšček, J. Park, *J. Power Sources* **2020**, *480*, 228742.
[21] a) J. Guo, A. Sun, X. Chen, C. Wang, A. Manivannan, *Electrochim. Acta* **2011**, *56*, 3981–3987; b) S. J. An, J. Li, C. Daniel, D. Mohanty, S. Nagpure, D. L. Wood, *Carbon* **2016**, *105*, 52–76.
[22] A. K. Stephan, *Joule* **2019**, *3*, 1812–1814.
[23] E. Ventosa, *Curr. Opin. Electrochem.* **2021**, *25*, 100635.
[24] T. Tarnev, P. Wilde, A. Dopilka, W. Schuhmann, C. K. Chan, E. Ventosa, *ChemElectroChem* **2020**, *7*, 665–671.
[25] E. Ventosa, W. Schuhmann, *Phys. Chem. Chem. Phys.* **2015**, *17*, 28441–28450.
[26] B. Liu, A. J. Bard, C.-Z. Li, H.-B. Kraatz, *J. Phys. Chem. B* **2005**, *109*, 5193–5198.
[27] A. Schilling, J. Schmitt, F. Dietrich, K. Dröder, *Energy Technol.* **2016**, *4*, 1502.
[28] C. S. Santos, A. Botz, A. S. Bandarenka, E. Ventosa, W. Schuhmann, *Angew. Chem. Int. Ed.* **2022**, *61*, e202202744.
[29] E. Ventosa, P. Wilde, A.-H. Zinn, M. Trautmann, A. Ludwig, W. Schuhmann, *Chem. Commun.* **2016**, *52*, 6825–6828.
[30] H. Bülter, M. Sternad, E. d Santos Sardinha, J. Witt, C. Dosche, M. Wilkening, G. Wittstock, *J. Electrochem. Soc.* **2016**, *163*, A504–A512.
[31] S. Klink, D. Höche, F. La Mantia, W. Schuhmann, *J. Power Sources* **2013**, *240*, 273–280.
[32] S. Klink, E. Madej, E. Ventosa, A. Lindner, W. Schuhmann, F. La Mantia, *Electrochem. Commun.* **2012**, *22*, 120–123.
[33] C. Lefrou, R. Cornut, *ChemPhysChem* **2010**, *11*, 547–556.
[34] C. M. Sánchez-Sánchez, J. Rodríguez-López, A. J. Bard, *Anal. Chem.* **2008**, *80*, 3254–3260.
[35] E. Ventosa, B. Paulitsch, P. Marzak, J. Yun, F. Schiegg, T. Quast, A. S. Bandarenka, *Adv. Mater. Interfaces* **2016**, *3*, 1600211.
[36] C. O. Laoire, E. Plichta, M. Hendrickson, S. Mukerjee, K. M. Abraham, *Electrochim. Acta* **2009**, *54*, 6560–6564.

Manuscript received: March 26, 2023
Revised manuscript received: May 28, 2023
Accepted manuscript online: June 1, 2023
Version of record online: June 26, 2023